Supporting Information for

Temperature controls the episodic dynamics of deep slow slip

Zaccaria El Yousfi, Baptiste Rousset, Mathilde Radiguet, and William B. Frank

Zaccaria El Yousfi
E-mail: zaccaria.el-yousfi@univ-grenoble-alpes.fr

This PDF file includes:

Materials and Methods

Quantifying low-frequency earthquake activity across four plate boundaries. We study low-frequency earthquake activity at each plate boundary using catalogs built with matched-filter searches, where each catalog is composed of event families that share similar waveforms characteristic of a specific source mechanism and location. We analyzed catalogs of low-frequency earthquakes in the subduction zones of Nankai (1), northern Cascadia (2), and Guerrero (3), as well as the Parkfield section of the San Andreas fault(4).

Given that our goal is to analyze the depth variations of low frequency earthquakes, we selected a subset of families to analyze in the Nankai and Parkfield catalogs. For the Nankai catalog, we only analyzed the families in the Shikoku region as they span larger depth ranges than other regions further to the northwest, such as the Kii Peninsula. For the Parkfield catalog, we kept the families located northwest of the city of Parkfield as they are located closer to the high-resolution seismic network, leading to better resolved depth estimations (4). As the catalogs of Guerrero and Parkfield respectively include a large slow slip event and an earthquake, we trim the catalog of Guerrero from the period (04/2006 - 09/2006) and the catalog of Parkfield from the period before 2006 (5). Depths of low-frequency earthquake sources are often poorly constrained due to low signal-to-noise ratios (3, 6). Additionally, differences in the approach used to locate the sources in each of the regions could imply systematic differences in the estimated depths. We therefore vertically projected every subduction zone low-frequency earthquake family onto slab models (7, 8); we used a global slab compilation for Guerrero and Cascadia (8) and a regional model for Nankai (7). For the Parkfield section of the San Andreas transform plate boundary, we used the reported depth of low-frequency earthquake families assuming a vertical fault geometry. Fig. S3 shows the observed depth distribution of low-frequency earthquakes across all four regions.

We quantify the activity of each low-frequency earthquake family in every catalog by computing an hourly event count time series; an example is shown in Fig. 2A. These event count time series capture the temporal evolution of low-frequency earthquake activity and highlight recurring swarms of low-frequency earthquakes (9). To estimate the average seismic behavior at a given depth, we spatially regroup families of low-frequency earthquakes at similar depths. We do this for each region by summing all the event count time series within ∼5-km depth bins to produce depth-dependent averages of low-frequency earthquake behavior.

Measuring low-frequency earthquake swarm durations. We use the depth-averaged low-frequency earthquake event count time series to compute autocorrelation functions for each bin of low-frequency earthquakes. The autocorrelation of the event count time series captures at short time lags the duration of low-frequency earthquake swarms (10, 11). We quantify the average duration of these swarms as the width of the autocorrelation's central peak. To estimate the width of the central autocorrelation peak, we first compute the baseline noise of the autocorrelation function as the average amplitude for time lags greater than 100 days, indicated by dark and light dashed purple lines in the inset in Fig. 2B. We then define a threshold at twice this average value and identify the shortest time lag at which the autocorrelation amplitude falls below this threshold, marked by dark and light purple squares in Fig. 2B. The optimal threshold is chosen by analyzing the durations obtained for a range of multiples of the baseline noise, shown in Fig. S5. We select the threshold as the compromise at the intersection between: (1) longer durations associated with noise in the autocorrelation tail and (2) shorter durations within the central autocorrelation peak (Fig. S5).

Measuring low-frequency earthquake swarm recurrence intervals. While it is possible to measure the recurrence interval of low-frequency earthquake swarms within the time domain of the autocorrelation functions, the quasi-periodic nature of the recurrence interval naturally lends itself to being quantified in the frequency domain. We thus developed a spectral-based method to estimate the average recurrence interval of low-frequency earthquakes within a given depth range. We first compute the Fourier spectrum of the event count autocorrelation with a multi-tapering approach (12); this is equivalent to computing the power spectral density of the event count time series. For a single taper v_k, the amplitude spectrum $\mathcal{F}_k$ as a function of the frequency ξ is defined as:

$$\mathcal{F}_k(\xi) = \int_{-\infty}^{\infty} \mathcal{R}(\tau)\, v_k\, e^{-i2\pi\xi\tau}\, d\tau, \qquad [1]$$

and the multi-taper estimate of the Fourier amplitude spectrum $\mathcal{F}_T(\xi)$ is:

$$\mathcal{F}_T(\xi) = \frac{\sum_{k=0}^{K-1} w_k |\mathcal{F}_k(\tau)|}{\sum_{k=0}^{K-1} w_k}, \qquad [2]$$

where w_k are normalization weights computed using the eigenvalues of the tapers, K is the tapering degree, and τ is the lag time axis. Higher values of the tapering degree K lead to a smoother spectrum spectrum (12); we use a tapering degree of 5 for the spectra presented in Figs. 2C, S1, and S2. The computed spectra are smoothed using a simple boxcar product (20-sample window) to remove the remaining short-period noise and focus on the recurrence intervals of the characteristic low-frequency earthquake swarms. Examples of spectra for deep and shallow low-frequency earthquake families in the Nankai subduction are shown in Fig. 2C.

To systematically estimate the average recurrence interval within each depth bin of low-frequency earthquake families, we compute the gradient of the spectra to identify the inflection point of the spectra, as shown by the color gradient in Fig. S1 and

retrieve the visible zero crossing of the gradient (Figs. 2 and S2). The computed multi-taper spectra and estimated recurrence intervals for all low-frequency earthquake families in all regions are shown in Fig. S2.

Uncertainties of recurrence interval and duration measurements. We estimate the uncertainty of our measures of duration and recurrence interval of low-frequency earthquake swarms through a jackknife approach. We do this by randomly resampling every measured time scale with a random subset of the low-frequency earthquake families in a given depth bin 100 times. We use the inter-quartile range (from 25% to 75%) of the duration and recurrence interval estimates in each depth bin in each region as the associated uncertainty. Then evaluate how the uncertainty varies as a function of the percentage families selected (Fig. S4). We select 75% as a compromise between a reasonable estimate of uncertainty while retaining a majority of our data in each random instance. We do not estimate uncertainties for the time scales measured from the Cascadia data because there is only one family per depth bin (2) (Fig. 1A).

Measuring low-frequency earthquake episodicity. Our model of episodic fault motion predicts that, for a given family of low-frequency earthquakes, the clustered fraction of events should occur within a duration shorter than $(D/R)T$, where T is the total time coverage of a given regional catalog. We refer to the fraction of low-frequency earthquakes that occur within this fraction of time as the episodicity; a value of 1 implies a low-frequency earthquake source that only produces events during regularly recurring episodes with no activity in between episodes. To estimate the episodicity for a low-frequency earthquake family, we compute the inter-event times of events within that family, sort the inter-event times in ascending order, and calculate their cumulative sum (see Fig. S7A). We measure the episodicity as the ratio of n/N, where n is the number of events that occur in less time than $(D/R)T$ and N is total number of low-frequency earthquakes in that family.

We observe that all low-frequency earthquake families exhibit episodicities of more than 65% with no resolvable systematic variation in depth (Fig. S7C). This suggests that low-frequency earthquake activity across all four plate boundaries is episodic, and most activity occurs within regularly recurring event swarms. While there appears to be some systematic trend towards higher episodicities at greater depths, this variation remains within measurement uncertainties. Higher episodicities at greater depths would suggest that slow slip becomes less episodic with depth, implying that there is less slip in between the characteristic slip episodes whose durations and recurrence we quantify. As durations and recurrence intervals decrease with depth, it is also possible that we approach the resolution limit of our measurements. The hourly time bins we use to estimate the event count time series means that we cannot resolve durations from the event count autocorrelations shorter than several hours. This creates the possibility for a bias in our estimates of episodicities at greater depths, as it becomes more challenging to reliably distinguish variations in slow slip dynamics from the average depth-dependent behavior. For these reasons, we do not interpret the variations of episodicity with depth.

A model of episodic slow slip and creep. Our measurements of episodicity suggest that only 65-95% (Fig. S7C) of the total long-term fault motion is accommodated by slow slip. This implies that the remaining budget of fault motion is taken up by creep in between slow slip events, which we call here inter-episode creep. We revisit here our model of episodic slow slip to quantitatively evaluate how our estimates of slow slip rate in Fig. 4 would change if we take into account the observed episodicities, which are inversely proportional to the potential amount of inter-episode creep.

The underlying assumption of our model of episodic slow slip is balancing the budget of fault motion, where each side of equation 1 has units of length (e.g., DV_S). To incorporate inter-slow slip creep, we rewrite the episodic slip model (eq. 1 in the article text) in terms of fault motion over one recurrence interval R:

$$u_S + u_C = u_L, \tag{3}$$

where u_S is the motion due to slow slip, u_C is the motion due to inter-episode creep, and u_L is the total long-term fault motion. We can relate this new form of our episodic slow slip model to the eq. 1 in the article with the following relations:

$$u_L = RV_L, \tag{4}$$
$$u_S = DV_S, \tag{5}$$
$$u_C = (R-D)V_C, \tag{6}$$

where the third term describes fault motion at the inter-episode creep rate V_C in the remainder of the recurrence interval $R - D$ when no slow slip is occurring.

Returning to our definition of the episodicity e of a low-frequency earthquake family (see previous paragraph), an episodicity of $e = 1$ suggests that 100% of the fault motion occurs during slow slip. An episodicity of $e < 1$ implies that $(1 - e)$% of fault motion is potentially accommodated by inter-episode creep. With this in mind, we can relate the terms for motion during slow slip u_S and inter-episode creep u_C to the episodicity e and the total fault motion u_L:

$$u_S = eu_L \tag{7}$$
$$u_C = (1-e)u_L. \tag{8}$$

We can then plug these two relations into equations 4-6 to obtain equations that relate the measured duration D and recurrence interval R time scales of slow slip to the long-term fault motion that is now scaled by the episodicity e:

$$DV_S = eRV_L \tag{9}$$
$$(R-D)V_C = (1-e)RV_L. \tag{10}$$

Focusing on V_S, we can now estimate slow slip rates as a function of the observed episodicity:

$$V_S = e\frac{R}{D}V_L. \quad [11]$$

We observe that in the presence of inter-episode creep, our model predicts a slow slip rate scaled by their episodicity e. This suggests that if we were to take into account the observed episodicities (Fig. S7), the slow slip rates predicted by our model of episodic slip would be ∼20% lower than those obtained at first order (eq. 1 in the main article text). While slightly lower, such slow slip rates are still entirely consistent with our interpretation and would still be consistent with geodetic models of slow slip (Table S7).

Thermal plate boundary models. We use thermal models to estimate the temperature at which low-frequency earthquake sources are observed. Every thermal model in Fig. 4D provides the temperature of the plate boundary as a function of pressure (13–16). We must therefore first compute the pressure of each low-frequency earthquake source to find the corresponding temperature. We estimate the pressure using the 1-D seismic AK135 model (17) for continental crusts and compute the pressure as $p = \int \rho(z)gdz$, where $\rho(z)$ is the depth-dependent density given by the AK135 model, $g = 9.81$ m/s^2 is the gravitational acceleration, and z are the bin depths we use to measure the average time scales of low-frequency earthquake swarms. We then convert the estimated pressures of low-frequency earthquake sources to the temperatures predicted by the thermal models (Fig. 4).

Supplementary figures

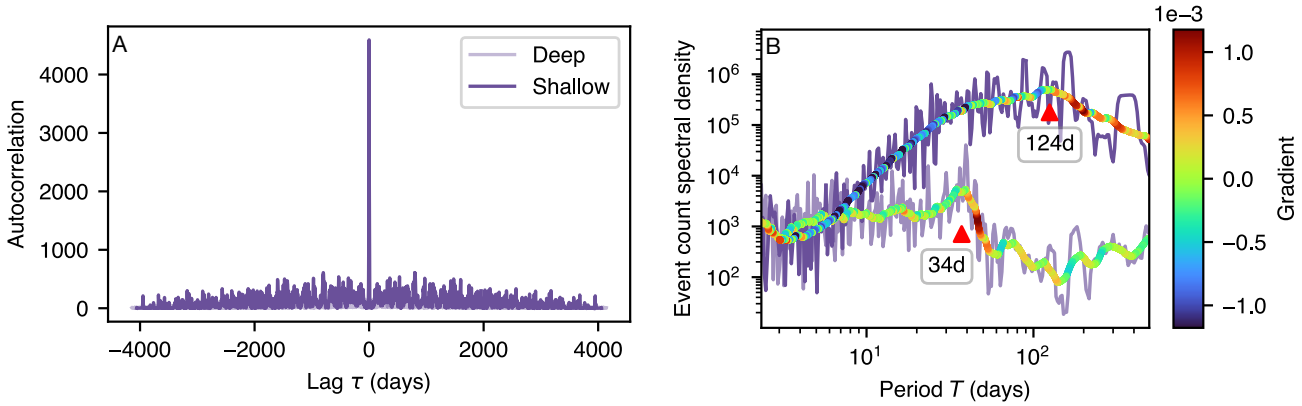

Figure S1. Measuring the recurrence interval of low-frequency earthquake swarms in the spectral domain. (A) Autocorrelation of the event count time series of the low-frequency earthquake families shown in Fig. 2. (B) Power spectral density of the event count autocorrelations in A. The purple curves are the multi-tapered Fourier transform (12) and multicolor curves are the smoothed spectrum colored by its gradient. We estimate the recurrence interval as the maximum of the spectrum, identified by the major zero crossing of the smoothed gradient.

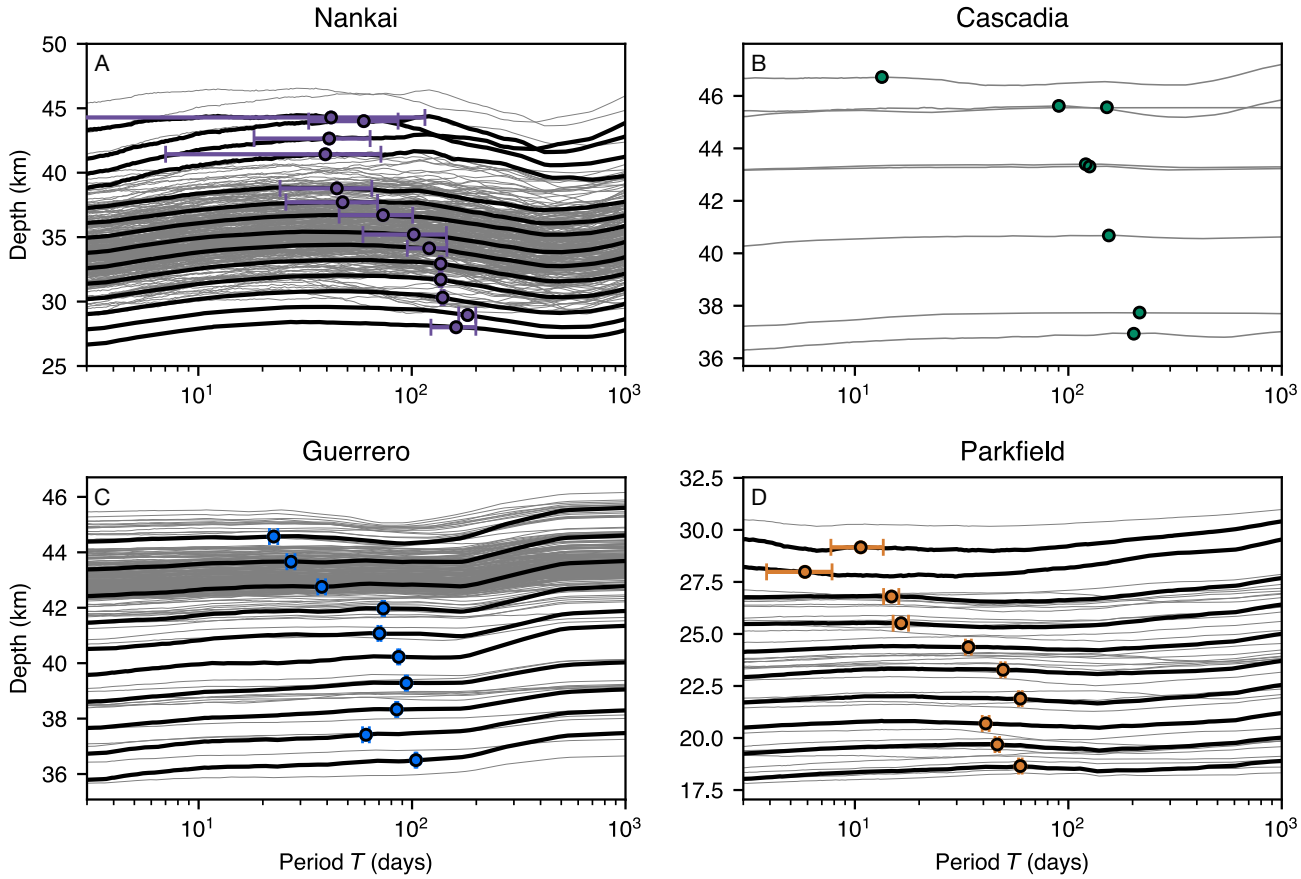

Figure S2. Systematic variation of low-frequency earthquake swarm recurrence intervals. Recurrence intervals are estimated as described in Materials and Methods and shown in Fig. S1. (A-D) Event count spectral densities and estimated recurrence intervals in all four regions: Nankai (A), Cascadia (B), Guerrero (C), and Parkfield (D). The spectra are sorted by the estimated depth of every low-frequency earthquake family. The grey curves are the individually estimated spectra, and the black curves represent the spectra estimated for each the depth bins. The points with the uncertainty bars represent the recurrence interval estimated for each of the depth bins.

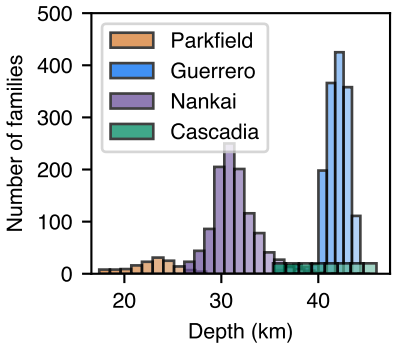

Figure S3. Depth distribution of low-frequency earthquake sources in every studied region. For Cascadia, single families are shown to represent the depth range of the catalog.

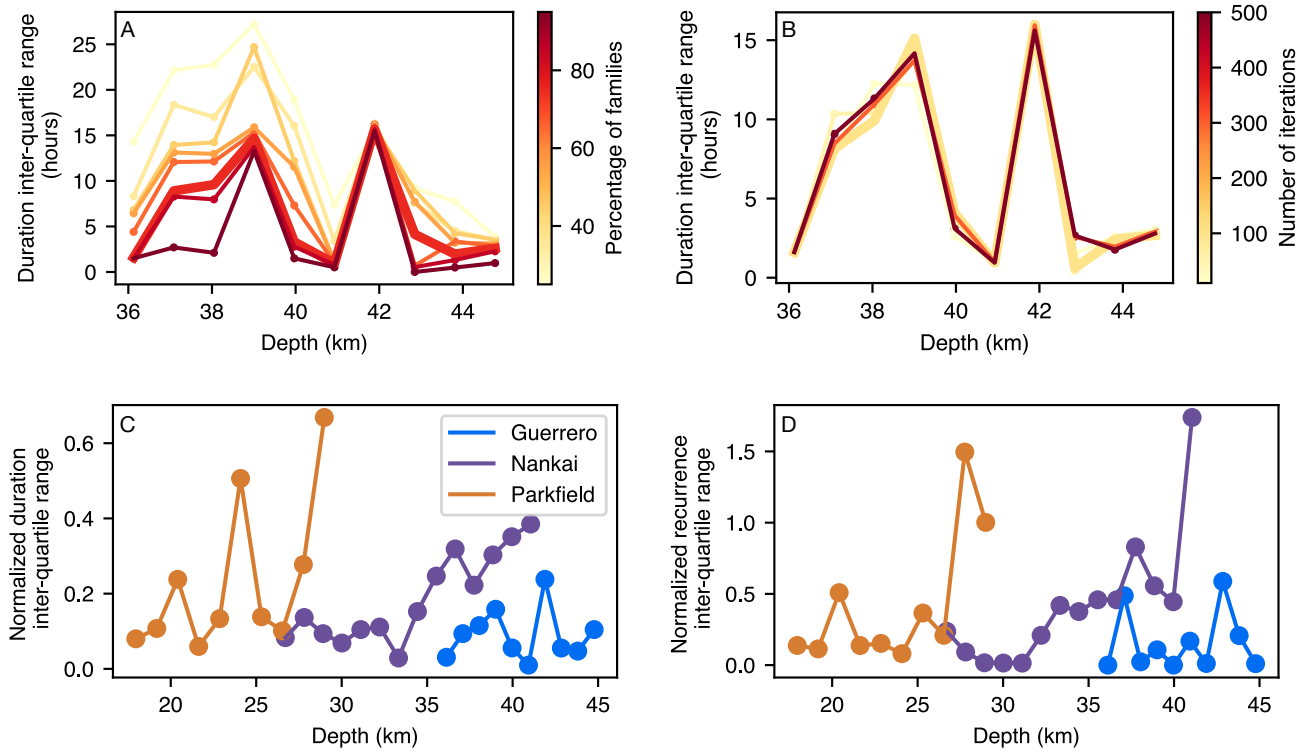

Figure S4. Uncertainty estimation of the duration and recurrence interval of low-frequency earthquake swarms with a jackknife approach. (A) Colored curves show the inter-quartile range (IQR) as a function of depth for several random subset fractions used for the jackknife analysis, shown by the colors. (B) Colored curves show the IQR as a function of depth for several numbers of random instances, shown by the colors. (C) IQRs normalized by the estimated durations as a function of depth. (D) IQRs normalized by the estimated recurrence intervals as a function of depth.

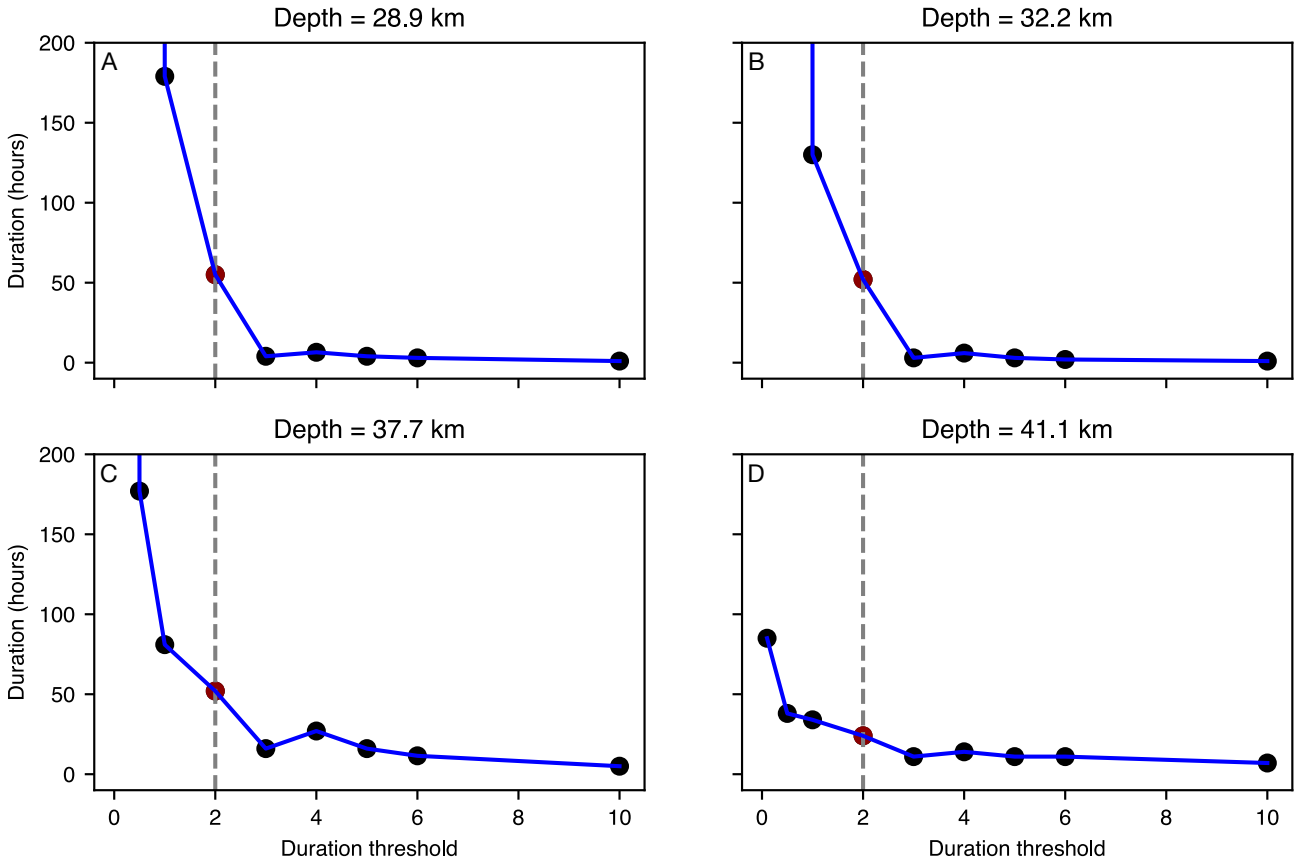

Figure S5. Estimates of low-frequency earthquake swarm durations as a function of the detection threshold. The threshold is a multiple of the average autocorrelation noise beyond 100 days of lag time (e.g., Fig. 2B and S1A). Panels A-D correspond to four depth bins in the Nankai subduction zone. The dark red points and the vertical dashed lines indicate the selected thresholds and durations for each low-frequency earthquake depth bin.

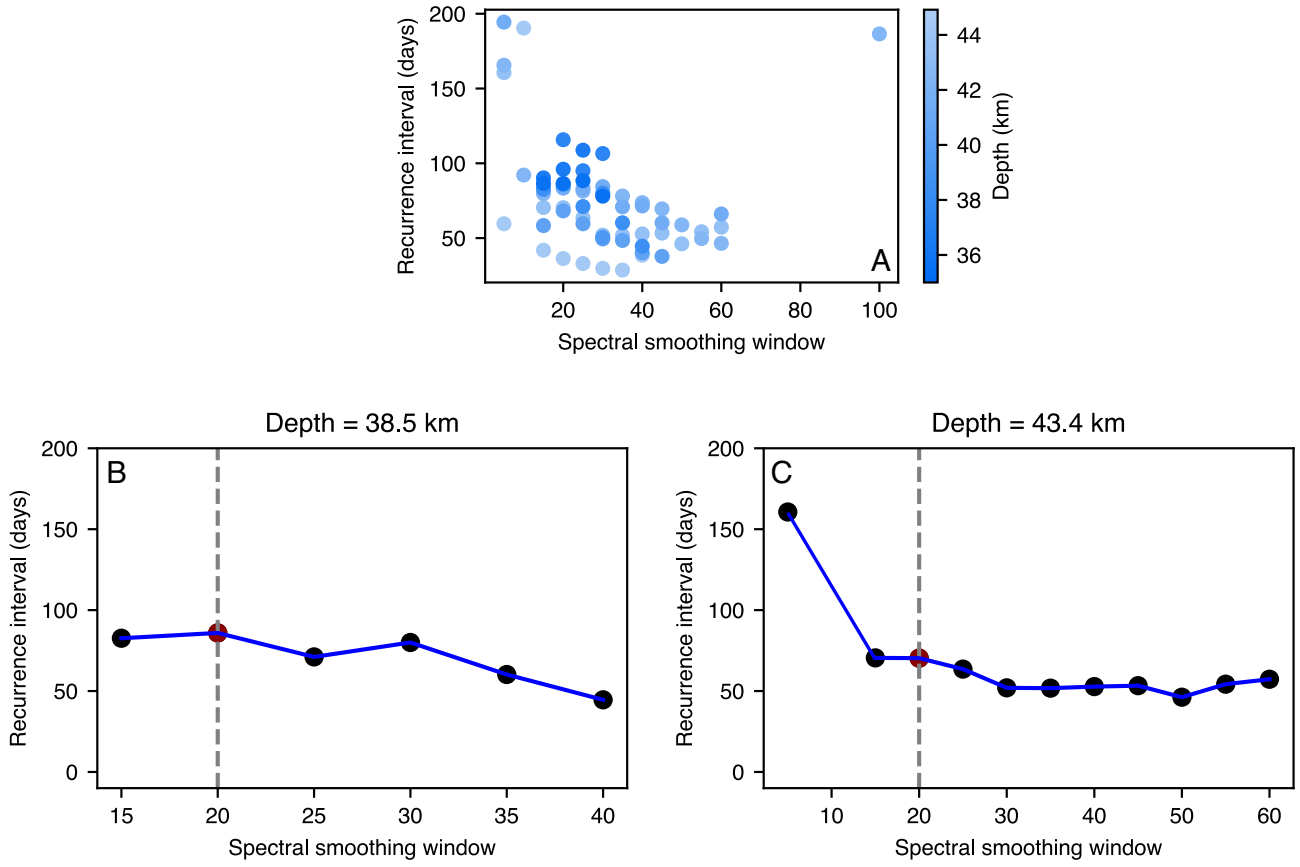

Figure S6. Impact of spectra smoothing on estimates of low-frequency earthquake swarm recurrence intervals in the Nankai subduction zone. (A) Colored dots show the low-frequency earthquake recurrence time as a function of the smoothing window applied to the event count spectral density. The depth of the low-frequency earthquake bin is shown by the colors. (B & C) Estimated recurrence intervals are shown as a function of the smoothing window size for two depth bins, a deep bin (B) and a shallow bin (C). The dark red points and the vertical dashed lines indicate the selected spectral smoothing window and recurrence at each low-frequency earthquake bin.

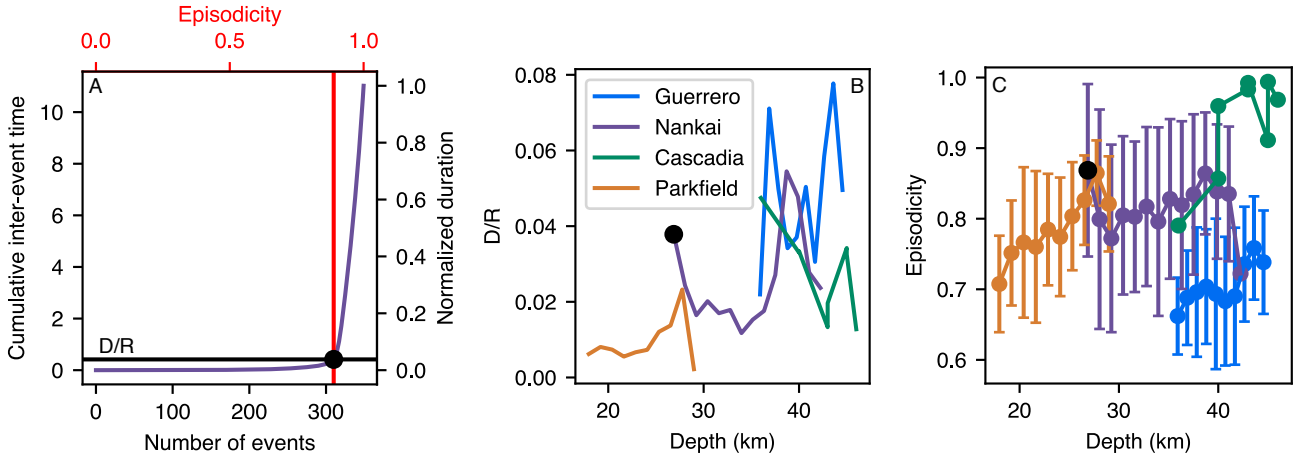

Figure S7. Measuring the episodicity of low-frequency earthquake activity (see Materials and Methods). (A) The purple curve shows the cumulative inter-event recurrence intervals for a low-frequency earthquake family in the Nankai subduction. The black line shows the expected fraction of time that low-frequency earthquakes are active, computed as the duration D over the recurrence interval R. The vertical red line indicates the fraction of events that occur within D/R fraction of the total time period, which corresponds to the estimated episodicity. (B) The curves D/R as a function of depth for each region in the same colors. (C) Colored points show the episodicity of every low-frequency earthquake depth bin in: Parkfield (orange), Nankai (purple), Guerrero (blue), and Cascadia (green); uncertainties are estimated as the inter-quartile range in each depth bin.

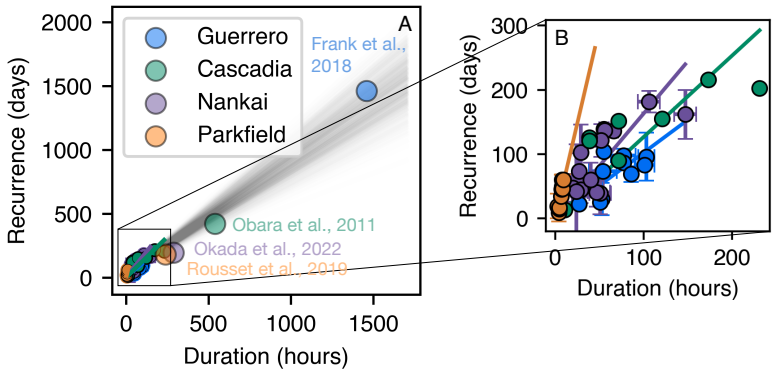

Figure S8. Slow slip durations as a function of their recurrence intervals, including both our observations (Fig. 3C) and geodetically-constrained slow slip events. (A) The small colored dots are recurrence intervals and durations for deep slow slip characterized in this study (Fig. 3C). The large colored dots are from geodetic estimates in Cascadia (18), in Guerrero (11), in Nankai (19), and in Parkfield (20). (B) Shows a zoom on the recurrence-duration space that contains our observations with trends computed as weighted orthogonal distance regressions, as shown in Fig. 3C.

Supplementary tables

Depth (km)	Temperature (°C)	Recurrence interval (days)	IQR (days)	Duration (hours)	IQR (hours)
26.70	387.19	161.73	38.32	147	12.41
27.81	395.01	181.57	16.72	106	12.52
28.91	402.66	139.18	2.27	55	5.28
30.02	410.25	136.29	1.99	66	5.21
31.12	417.44	137.29	1.94	56	6.37
32.22	424.49	121.30	25.37	52	5.55
33.33	431.63	102.93	43.14	29	0.73
34.43	438.08	73.55	27.64	27	3.80
35.53	444.38	47.36	21.71	20	5.11
36.64	450.73	44.56	20.42	29	8.36
37.74	457.09	38.97	32.33	51	12.22
38.85	462.82	40.94	22.79	47	15.10
39.95	468.31	60.02	26.70	40	14.87
41.05	473.42	42.22	73.39	24	12.47

Table S1. Measured low-frequency earthquake swarm recurrence intervals and durations for the Nankai subduction zone and associated uncertainties. Temperatures are estimated with a regional thermal model (13). The listed depths are the averages of the spatial bins in which we group together low-frequency earthquakes at similar depths (see Materials and Methods). Uncertainty is estimated as the inter-quartile range (IQR) of each depth bin using a jackknife approach (see Materials and Methods).

Depth (km)	Temperature (°C)	Recurrence interval (days)	IQR (days)	Duration (hours)	IQR (hours)
36.13	422.98	104.34	0.00	55	1.71
37.09	437.04	96.03	37.08	103	9.27
38.05	498.38	83.05	1.93	101	11.05
39.01	508.23	98.04	10.13	77	13.72
39.97	514.35	86.57	/	77	4.30
40.93	518.90	68.91	12.12	86	0.86
41.89	523.04	73.33	0.85	54	15.78
42.85	526.44	30.05	25.10	53	2.95
43.81	529.87	25.46	5.74	51	2.36
44.77	533.19	22.48	0.23	27	2.73

Table S2. Measured low-frequency earthquake swarm recurrence intervals and durations for the Guerrero subduction zone and associated uncertainties. Temperatures are estimated with a regional thermal model (14). The listed depths are the averages of the spatial bins in which we group together low-frequency earthquakes at similar depths (see Materials and Methods). Uncertainty is estimated as the inter-quartile range (IQR) of each depth bin using a jackknife approach (see Materials and Methods).

Depth (km)	Temperature (°C)	Recurrence interval (days)	Duration (hours)
36	462.43	202.64	231
45	498.05	90.25	71
46	501.76	13.38	11
43	490.42	125.75	38
43	490.42	120.64	38
45	498.05	151.57	71
40	478.99	154.74	121
37	466.58	215.65	173

Table S3. Measured low-frequency earthquake swarm recurrence intervals and durations for the Cascadia subduction zone. Temperatures are estimated with a regional thermal model (13). Uncertainties are not measured for Cascadia as each low-frequency earthquake source was analyzed individually.

Depth (km)	Temperature (°C)	Recurrence interval (days)	IQR (days)	Duration (hours)	IQR (hours)
28.98	640.30	19.08	19.12	2.99	2.00
27.76	616.60	8.96	13.39	4.42	1.23
26.53	592.90	15.16	3.17	5.02	0.51
25.31	565.30	17.25	6.31	4.96	0.69
24.08	535.50	34.21	2.74	6.89	3.49
22.86	505.30	49.98	7.62	7.59	1.01
21.63	474.80	60.31	8.29	7.82	0.47
20.41	443.90	45.20	23.00	7.42	1.77
19.18	423.10	46.44	5.28	8.47	0.91
17.96	391.60	60.42	8.34	9.28	0.74

Table S4. Measured low-frequency earthquake swarm recurrence intervals and durations for the Parkfield section of the San Andreas fault and associated uncertainties. Temperatures are estimated with a regional thermal model (15). The listed depths are the averages of the spatial bins in which we group together low-frequency earthquakes at similar depths (see Materials and Methods). Uncertainty is estimated as the inter-quartile range (IQR) of each depth bin using a jackknife approach (see Materials and Methods).

	Guerrero	Nankai	Cascadia	Parkfield
R/D	24.5±2.6	39.1±4.1	30.5±4.3	141.4±17.0
V_L	65 (21)	65 (19)	43 (22)	34 (23)
V_S	4.4±0.5	6.9±0.7	3.6±0.5	13.2±1.6

Table S5. Estimated regional trends (R/D) of recurrence and duration (Fig. 3C), using an orthogonal distance regression that takes into account the observational uncertainties of both R and D. The second and third rows are respectively the used long-term plate motion rates V_L in mm/yr and the predicted slow slip rates V_S in mm/day.

Guerrero	Nankai	Cascadia	Parkfield
8.1	4.7	2.5	14.2
3.9	7.3	3.6	4.5
3.5	10.8	3.4	6.7
5.4	8.8	9.2	7.8
4.8	10.5	8.9	11.1
3.4	9.9	5.9	14.7
5.8	15.2	3.6	17.2
2.4	11.6	3.5	13.6
2.1	10.1		12.2
3.6	6.6		14.5
	3.3		
	3.7		
	6.4		
	7.5		

Table S6. Compilation of deep slow slip rates (mm/day) for the studies regions that are shown in Fig. 4A & B, see depths in Tab. S1,S2,S3, and S4 respectively.

Region	Slow slip depth	Slow slip rate (mm/day)	Reference
Guerrero	Deep	0.4, 0.4, 0.6, 0.5	(21, 24–26)
Cascadia	Deep	0.1, 0.6, 1.2, 2.0, 2.5	(22, 27–30)
Nankai	Deep	0.5, 0.3, 1.5	(19, 31, 32)
Boso	Shallow	12.5	(33)
Parkfield	Deep	0.4	(20)
Hikurangi	Deep	1.0	(34)
	Shallow	1.0, 10.0	(34, 35)
Alaska	Deep	3.0 , 2.0	(36, 37)
Ecuador	Shallow	1.3	(38)
Costa Rica	Shallow	5.5	(39)

Table S7. A compilation of geodetically-inferred slow slip rates across many plate boundaries, including the four we study here. We report the average slip rate if provided in the cited reference. Otherwise, we estimate slip rates by taking the ratio of the reported geodetically-inferred slip and the estimated slow slip duration. "Deep" indicates slow slip downdip of the seismogenic zone, while "shallow" indicates slow slip updip of the seismogenic zone.

References

1. Kato A, Nakagawa S (2020) Detection of deep low-frequency earthquakes in the nankai subduction zone over 11 years using a matched filter technique. *Earth, Planets and Space* 72(1):128.
2. Sweet JR, Creager KC, Houston H, Chestler SR (2019) Variations in cascadia low-frequency earthquake behavior with downdip distance. *Geochemistry, Geophysics, Geosystems* 20(2):1202–1217.
3. Frank WB, et al. (2014) Using systematically characterized low-frequency earthquakes as a fault probe in guerrero, mexico. *Journal of Geophysical Research: Solid Earth* 119(10):7686–7700.
4. Shelly DR (2017) A 15 year catalog of more than 1 million low-frequency earthquakes: Tracking tremor and slip along the deep san andreas fault. *Journal of Geophysical Research: Solid Earth* 122(5):3739–3753.
5. Shelly DR, Johnson KM (2011) Tremor reveals stress shadowing, deep postseismic creep, and depth-dependent slip recurrence on the lower-crustal san andreas fault near parkfield. *Geophysical Research Letters* 38(13).
6. Brown JR, et al. (2009) Deep low-frequency earthquakes in tremor localize to the plate interface in multiple subduction zones. *Geophysical Research Letters* 36(19).
7. Hirose F, Nakajima J, Hasegawa A (2008) Three-dimensional seismic velocity structure and configuration of the philippine sea slab in southwestern japan estimated by double-difference tomography. *Journal of Geophysical Research: Solid Earth* 113(B9).
8. Hayes GP, et al. (2018) Slab2, a comprehensive subduction zone geometry model. *Science* 362(6410):58–61.
9. Frank WB, et al. (2016) The evolving interaction of low-frequency earthquakes during transient slip. *Science Advances* 2(4):e1501616.
10. Frank WB (2016) Slow slip hidden in the noise: The intermittence of tectonic release. *Geophysical Research Letters* 43(19):10,125–10,133.
11. Frank WB, Rousset B, Lasserre C, Campillo M (2018) Revealing the cluster of slow transients behind a large slow slip event. *Science Advances* 4(5):eaat0661.
12. Prieto GA (2022) The Multitaper Spectrum Analysis Package in Python. *Seismological Research Letters* 93(3):1922–1929.
13. Peacock SM (2009) Thermal and metamorphic environment of subduction zone episodic tremor and slip. *Journal of Geophysical Research: Solid Earth* 114(B8).
14. van Keken PE, Wada I, Abers GA, Hacker BR, Wang K (2018) Mafic high-pressure rocks are preferentially exhumed from warm subduction settings. *Geochemistry, Geophysics, Geosystems* 19(9):2934–2961.
15. Gao X, Wang K (2017) Rheological separation of the megathrust seismogenic zone and episodic tremor and slip. *Nature* 543(7645):416–419.
16. Condit CB, Guevara VE, Delph JR, French ME (2020) Slab dehydration in warm subduction zones at depths of episodic slip and tremor. *Earth and Planetary Science Letters* 552:116601.
17. Kennett BLN, Engdahl ER, Buland R (1995) Constraints on seismic velocities in the earth from traveltimes. *Geophysical Journal International* 122(1):108–124.
18. Obara K (2011) Characteristics and interactions between non-volcanic tremor and related slow earthquakes in the nankai subduction zone, southwest japan. *Journal of Geodynamics* 52(3–4):229–248.
19. Okada Y, Nishimura T, Tabei T, Matsushima T, Hirose H (2022) Development of a detection method for short-term slow slip events using gnss data and its application to the nankai subduction zone. *Earth, Planets and Space* 74(1):18.
20. Rousset B, Bürgmann R, Campillo M (2019) Slow slip events in the roots of the san andreas fault. *Science Advances* 5(2).
21. El Yousfi Z, et al. (2023) Intermittence of transient slow slip in the mexican subduction zone. *Earth and Planetary Science Letters* 620:118340.
22. Bartlow NM (2020) A long-term view of episodic tremor and slip in cascadia. *Geophysical Research Letters* 47(3):e2019GL085303.
23. Ryder I, Bürgmann R (2008) Spatial variations in slip deficit on the central san andreas fault from insar. *Geophysical Journal International* 175(3):837–852.
24. Radiguet M, et al. (2012) Slow slip events and strain accumulation in the guerrero gap, mexico. *Journal of Geophysical Research: Solid Earth* 117(B4).
25. Graham S, et al. (2016) Slow slip history for the mexico subduction zone: 2005 through 2011. *Pure and Applied Geophysics* 173(10):3445–3465.
26. Frank WB, et al. (2015) Uncovering the geodetic signature of silent slip through repeating earthquakes. *Geophysical Research Letters* 42(8):2774–2779.
27. Michel S, Gualandi A, Avouac JP (2019) Similar scaling laws for earthquakes and cascadia slow-slip events. *Nature* 574(7779):522–526.
28. Itoh Y, Aoki Y, Fukuda J (2022) Imaging evolution of cascadia slow-slip event using high-rate gps. *Scientific Reports* 12(1):7179.
29. Bletery Q, Nocquet JM (2020) Slip bursts during coalescence of slow slip events in cascadia. *Nature communications* 11(1):2159.
30. Wech AG, Bartlow NM (2014) Slip rate and tremor genesis in cascadia. *Geophysical Research Letters* 41(2):392–398.
31. Nishimura T, Matsuzawa T, Obara K (2013) Detection of short-term slow slip events along the nankai trough, southwest japan, using gnss data. *Journal of Geophysical Research: Solid Earth* 118(6):3112–3125.
32. Takagi R, Uchida N, Obara K (2019) Along-strike variation and migration of long-term slow slip events in the western

nankai subduction zone, japan. *Journal of Geophysical Research: Solid Earth* 124(4):3853–3880.
33. Ozawa S, Yarai H, Kobayashi T (2019) Recovery of the recurrence interval of boso slow slip events in japan. *Earth, Planets and Space* 71(1):78.
34. Michel S, Jolivet R, Klein E, Maubant L (2025) 14 years of slip on the hikurangi subduction zone. *Journal of Geophysical Research: Solid Earth* 130(7).
35. Wallace LM, et al. (2016) Slow slip near the trench at the hikurangi subduction zone, new zealand. *Science* 352(6286):701–704.
36. Rousset B, Fu Y, Bartlow N, Bürgmann R (2019) Weeks-long and years-long slow slip and tectonic tremor episodes on the south central alaska megathrust. *Journal of Geophysical Research: Solid Earth* 124(12):13392–13403.
37. Okada Y, Nishimura T (2023) Systematic detection of short-term slow slip events in southcentral alaska. *Geophysical Research Letters* 50(17):e2023GL104901.
38. Vaca S, Vallée M, Nocquet JM, Battaglia J, Régnier M (2018) Recurrent slow slip events as a barrier to the northward rupture propagation of the 2016 pedernales earthquake (central ecuador). *Tectonophysics* 724:80–92.
39. Jiang Y, et al. (2017) Strain release at the trench during shallow slow slip: The example of nicoya peninsula, costa rica. *Geophysical Research Letters* 44(10):4846–4854.